Available online at www.sciencedirect.com

ScienceDirect

IFAC Papers Online CONFERENCE PAPER ARCHIVE

IFAC PapersOnLine 53-2 (2020) 9950–9955

Control of Sliding Velocity in Robotic Object Pivoting Based on Tactile Sensing ⋆

Marco Costanzo Giuseppe De Maria Ciro Natale

* *Università degli Studi della Campania Luigi Vanvitelli, Aversa, 81031 Italy (e-mail: {marco.costanzo,giuseppe.demaria,ciro.natale}@unicampania.it).*

Abstract: Control of robots manipulating objects using only the sense of touch is a challenge. In-hand motion of the manipulated object highly depends on the friction forces acting at the contact surfaces. Soft contacts allow torsional frictions as well as friction forces, therefore robots can perform more complex manipulation abilities, like object pivoting. Control of the pivoting sliding motion is very difficult especially without any visual feedback. The paper proposes a novel method to control the sliding velocity of the object by using a simple parallel gripper endowed with force/tactile sensors only. The strategy is based on a nonlinear observer that estimates the sliding velocity from force/torque measurements and a model of the sliding dynamics.

Keywords: Robotic manipulators, Robot control, Friction, Nonlinear systems, Observers.

1. INTRODUCTION

The ability of robots to manipulate objects of various shapes and materials is crucial for broadening their use in service robotics. For a number of years researchers focused their efforts in devising complex robotic hands with many degrees of freedom (Piazza et al., 2019). However, recent approaches proposed the adoption of more simple devices and the exploitation of external aids to enhance the gripper dexterity (Dafle et al., 2014). A typical task that can be performed even by a simple parallel gripper to change the pose of the grasped object without a re-grasping maneuver is the so-called *object pivoting*. It consists in allowing a controlled rotation of the grasped object subject to gravity by suitably acting on the grasping force. The task has been performed in different ways, e.g., by using both visual and tactile sensors by Viña et al. (2016) or even by using tactile sensors only by Costanzo et al. (2018). The first approach allows to control the object orientation owing to the visual feedback, while the tactile sensor is used to control the grasp force. In the second paper, force sensors on the fingertips are used for both grasp force control and for executing the pivoting maneuver with the limitation of the a priori knowledge of the initial orientation of the grasped object. Performing the pivoting task using the sole tactile feedback is very challenging even for a human and an accurate control of the object orientation is not possible. However, under some assumptions, clarified in the present work, it is possible to track a given velocity profile of the sliding motion, hence indirectly controlling the object angular position. However, the actual velocity can only be estimated from the tactile measurements and thus the accuracy in the final pose will be affected by the accuracy of some model parameters. Indeed, the control approach is based on a dynamic model of the object motion described as a pure rotational motion about the instantaneous center of rotation (CoR). Modelling friction torques is thus crucial and to this aim we adopt the soft contact dynamic model proposed by Costanzo et al. (2020). In that paper an Extended Kalman filter was used to estimate the sliding velocity with its usual convergence problems, which were solved by an accurate tuning of the filter covariance matrices and by resorting to a computationally demanding digital implementation based on the Runge-Kutta numerical integration method. Here, the velocity is estimated via a nonlinear observer with proved convergence. Experiments carried out on a Kuka LBR iiwa equipped with a sensorized gripper show the effectiveness of the nonlinear observer in estimating the sliding velocity as well as of the control strategy to track a given velocity profile.

2. DYNAMIC MODELING

This paper adopts the dynamic model proposed by Costanzo et al. (2020), it will be briefly described in this section highlighting some minor differences.

Consider a planar slider on which a hemispherical soft pad applies a friction force with components laying on a plane; the magnitude of the friction force can be controlled by acting on a force normal to the plane. Define a contact frame with the z axis normal to the contact surface in the direction of the normal load and the y axis along the direction of the tangential load. The origin of the contact frame is located in the Center of Pressure (CoP) of the contact area, that is circular in view of the soft pad shape. The pressure distribution is assumed axisymmetric with respect to the z axis.

Under such assumptions, the instantaneous rotational motion can be described by a twist vector with components in the contact frame

$$\boldsymbol{t} = [\, v_x \;\; v_y \;\; \omega_z \,]^T, \tag{1}$$

⋆ This work was supported by the European Commission within the H2020 REFILLS project, ID n. 731590.

10.1016/j.ifacol.2020.12.2710

where v_x and v_y are the components of the linear velocity and ω_z is the component of the angular velocity. Hence, as shown by Lynch and Park (2017), the CoR has position

$$\boldsymbol{p}_{\mathrm{CoR}} = [\, -v_y/\omega_z \;\; v_x/\omega_z \;\; 0 \,]^T, \tag{2}$$

that is orthogonal to $\boldsymbol{t}$.

By kinetostatic duality, the friction load acting on the soft pad can be represented by the three-dimensional wrench

$$\boldsymbol{w} = [\, 0 \;\; f_t \;\; \tau_n \,]^T, \tag{3}$$

with f_t and τ_n the tangential and torsional load, respectively. In view of the particular choice of the reference contact frame, the following constraints hold

$$f_t \geq 0, \;\; f_n \geq 0, \;\; \tau_n \lesseqgtr 0, \tag{4}$$

where f_n is the normal load, which is also the control input signal available to control the motion of the planar slider.

Under the assumption of axisymmetric pressure distribution, the CoR position is orthogonal to the direction of the wrench and thus $v_x = 0$ (Howe and Cutkosky, 1996). Therefore, the CoR position has components $[\, c \;\; 0 \;\; 0 \,]^T$, with

$$c = -v_y/\omega_z. \tag{5}$$

Moreover, in view of the load motion inequality (Goyal et al., 1991), c and τ_n have always opposite signs.

Since the instantaneous motion of the slider can be described as a pure rotation about the CoR, its dynamics can be described by the Euler equation

$$J\dot{\omega}_z = -\sigma_1\omega_z - \tau_f + \tau_e, \tag{6}$$

where J is the inertia moment of the slider about the CoR, σ_1 is the viscous friction coefficient, τ_f is the dry friction torque and τ_e is the external torque acting on the slider. The dry friction is modeled with the well-known LuGre model by Canudas de Wit et al. (1995), i.e.,

$$\dot{z} = \omega_z - \frac{\sigma_0}{g(f_n, c)} z|\omega_z| \tag{7}$$

$$\tau_f = \sigma_0 z, \tag{8}$$

where z is the LuGre state variable, i.e., the displacement of the micro asperities, $g(f_n, c)$ is the maximum dry friction torque that can be applied to the slider and σ_0 is the stiffness of the micro asperities. The classical LuGre model was devised for translational friction, while the slider considered in this paper is subject to both linear forces and torsional moments since the slider is subject to a soft distributed contact. Therefore, a new method to compute the maximum dry friction torque as a function of the normal force is necessary. A well-known approach to address this problem is the one based on the Limit Surface (LS) concept by Goyal et al. (1991).

The LS is the locus of the points $(f_{t_{LS}}, \tau_{n_{LS}})$ identified by the maximum tangential and torsional friction loads that can be withstood at the contact. The LS is usually represented normalized with respect to the maximum tangential and torsional friction loads that can be applied before slipping. These are related to the normal load through the relationships (Xydas and Kao, 1999)

$$f_{t_{\max}} = \mu f_n \tag{9}$$

$$\tau_{n_{\max}} = \mu\xi\delta f_n^{\gamma+1}, \tag{10}$$

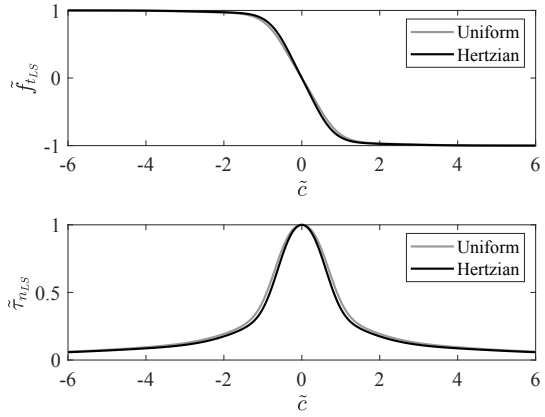

Fig. 1. Typical graphs (uniform and Hertzian pressure distributions) of $\tilde{f}_{t_{LS}}$ and $\tilde{\tau}_{n_{LS}}$ as functions of $\tilde{c}$.

where μ is the friction coefficient, ξ is a parameter depending on the pressure distribution on the contact area, while δ and γ are parameters, depending on the soft pad material, which relate the radius of the contact area ρ to the normal load as (Xydas and Kao, 1999)

$$\rho = \delta f_n^{\gamma}. \tag{11}$$

A point on the normalized LS can be computed according to the integrals (Xydas and Kao, 1999; Howe and Cutkosky, 1996) in polar coordinates (r, θ)

$$\tilde{f}_{t_{LS}} = \frac{1}{\pi}\int_0^{2\pi}\int_0^1 p'(\tilde{r})\frac{\tilde{r}(\tilde{r}\cos\theta - \tilde{c})}{\sqrt{\tilde{r}^2 + \tilde{c}^2 - 2\tilde{c}\tilde{r}\cos\theta}} d\tilde{r}d\theta \tag{12}$$

$$\tilde{\tau}_{n_{LS}} = \frac{1}{\pi\xi}\int_0^{2\pi}\int_0^1 p'(\tilde{r})\frac{\tilde{r}^2(\tilde{r} - \tilde{c}\cos\theta)}{\sqrt{\tilde{r}^2 + \tilde{c}^2 - 2\tilde{c}\tilde{r}\cos\theta}} d\tilde{r}d\theta, \tag{13}$$

where the function $p'(\tilde{r}) = \pi\rho^2/f_n p(r)|_{r=\rho\tilde{r}}$ is proportional to the pressure distribution $p(r)$ in the normalized variables $\tilde{r} = r/\rho$ and $\tilde{c} = c/\rho$. It can be shown that $p'(\tilde{r})$ does not depend on f_n.

Given the pressure distribution, the normalized tangential and torsional loads are functions of $\tilde{c}$. Hence, they can be computed only once by resorting to any universal approximator. Taking into account their typical shapes reported in Fig. 1, it is convenient to use a superposition of sigmoidal functions for $\tilde{f}_{t_{LS}}(\tilde{c})$ and of Gaussian functions for $\tilde{\tau}_{n_{LS}}(\tilde{c})$, which are both radial basis functions, i.e.,

$$\tilde{f}_{t_{LS}}(\tilde{c}) = \sum_{i=1}^{n} w_{f_i}\left(\frac{2}{1 + e^{a_i(\tilde{c} - m_{f_i})}} - 1\right) \tag{14}$$

$$\tilde{\tau}_{n_{LS}}(\tilde{c}) = \sum_{i=1}^{n} w_{\tau_i} e^{-\frac{(\tilde{c} - m_{\tau_i})^2}{2s_i^2}}, \tag{15}$$

where the weights w_{f_i}, w_{τ_i} and the parameters a_i, m_{f_i}, m_{τ_i}, s_i of the sigmoidal and Gaussian functions can be estimated via a nonlinear optimization based on the numerically computed integrals in (12) and (13). Note that all pressure distributions defined by Xydas and Kao (1999) are such that the functions $\tilde{f}_{t_{LS}}$ and $\tilde{\tau}_{n_{LS}}$ have graphs contained within the two reported in Fig. 1. This demonstrates the weak sensitivity of both functions with respect to pressure distribution. This method to compute the LS through approximators is the main difference of the

static model proposed here compared to that presented by Costanzo et al. (2020) and it will be used to compute the maximum static friction torque given the normal load.

The dynamic model describes the motion as a pure instantaneous rotation about the CoR. Thus, it is important to estimate the CoR position c (or equivalently $\tilde{c}$). By using the approximators (14)-(15), given a load (f_t, τ_n), $\tilde{c}$ is the solution of the following nonlinear equation

$$\sigma = \frac{|\tilde{f}_{t_{LS}}(\tilde{c})|^{\gamma+1}\text{sign}(\tilde{f}_{t_{LS}}(\tilde{c}))}{\tilde{\tau}_{n_{LS}}(\tilde{c})}, \quad \text{where } \sigma = \frac{\xi\delta}{\mu^\gamma}\frac{f_t^{\gamma+1}}{\tau_n}. \tag{16}$$

It can be solved by resorting to any nonlinear solver, e.g., Newton's method. Note that the $|\cdot|$ and the sign$(\cdot)$ functions are needed to make the functions $\tilde{f}_{t_{LS}}(\tilde{c})$ and $\tilde{\tau}_{n_{LS}}(\tilde{c})$ compatible with the constraints (4).

In summary, the maximum dry friction torque that can be produced at the contact surface given the normal load f_n and the instantaneous CoR position c can be computed by summing up the pure torsional moment $\tau_{n_{LS}}$ with the moment of the tangential force $f_{t_{LS}}$ about the CoR

$$g(f_n, c) = |\tau_{n_{LS}}| + |c f_{t_{LS}}|. \tag{17}$$

Note that $g > 0$ since $\tau_{n_{LS}}$ and $f_{t_{LS}}$ cannot be both zero provided that $f_n > 0$. Computing g in (17) requires computation of $f_{t_{LS}}$ and $\tau_{n_{LS}}$ according to the procedure

- Compute the CoR position $\tilde{c}$ by solving the nonlinear equation (16)
- Compute $\tilde{f}_{t_{LS}}$ and $\tilde{\tau}_{n_{LS}}$ using (14) and (15)
- Denormalize using (9) and (10)

3. CONTROL OF THE SLIDING VELOCITY

3.1 Control objective and preliminaries

The control objective is to follow a given velocity profile $\omega_d(t)$ by acting on the normal force and thus on the friction torque τ_f. First of all, such objective can be achieved only in presence of an external torque such that $|\tau_e| > g$, where the arguments of the function g have been omitted for brevity. To prove this, we start by computing the equilibrium points of the system (6) and (7), i.e., with τ_e and g constant values. With a disturbance torque $|\tau_e| < g$ the only equilibrium point is

$$\begin{pmatrix} \bar{\omega}_z \\ \bar{z} \end{pmatrix} = \begin{pmatrix} 0 \\ \tau_e/\sigma_0 \end{pmatrix}. \tag{18}$$

In fact, any other solution would imply $\sigma_0 z = g\,\text{sign}(\omega_z)$, resulting in $\text{sign}(\omega_z) = \text{sign}(\tau_e/g - \text{sign}(\omega_z))$, that is impossible when $|\tau_e|/g < 1$.

When the disturbance torque is such that $|\tau_e| > g$, then we have two equilibrium points. One is still (18), and the other one is

$$\begin{pmatrix} \bar{\omega}_z \\ \bar{z} \end{pmatrix} = \begin{pmatrix} (\tau_e - g\text{sign}(\tau_e))/\sigma_1 \\ g\text{sign}(\tau_e)/\sigma_0 \end{pmatrix}. \tag{19}$$

The equilibrium point (18) of the dynamic system (6) and (7) can be shown to be asymptotically stable for any $|\tau_e| < g$. The proof, based on the Lyapunov method, is out of the scope of this paper, which focuses on the situation where the slider moves, i.e., $\omega_z \neq 0$. Nevertheless, this result means that controlling the velocity is meaningful only for $|\tau_e| > g$. In such a case, the state (18) is still an equilibrium, but it can be shown to be unstable.Whereas, the equilibrium (19) is proved to be locally asymptotically stable in the following proposition.

Proposition 1. The equilibrium point (19) of the dynamic system (6) and (7) is locally asymptotically stable for any $|\tau_e| > g$.

Proof. We will present the proof for $\tau_e < -g$ and thus $\bar{\omega}_z < 0$, which is the case considered in the experiments of Section 4, but the case $\tau_e > g$ is similar. The jacobian of the linearized system around the equilibrium is

$$\begin{pmatrix} -\sigma_1/J & -\sigma_0/J \\ 1 + \sigma_0\bar{z}/g & -\sigma_0|\bar{\omega}_z|/g \end{pmatrix} = \begin{pmatrix} -\sigma_1/J & -\sigma_0/J \\ 0 & -\sigma_0|\tau_e + g|/(g\sigma_1) \end{pmatrix},$$

that is trivially Hurwitz.

A generalization of this result is obtained by considering a time varying external torque $\tau_e(t)$ but such that $|\tau_e(t)| > g$, $\forall t \geq 0$. Note that this assumption implies that the $\tau_e(t)$ has constant sign, denote the sign(τ_e) with s_τ. Under such assumptions and with the initial condition

$$\begin{pmatrix} \omega_z(0) \\ z(0) \end{pmatrix} = \begin{pmatrix} \omega_0 s_\tau \\ g/\sigma_0 s_\tau \end{pmatrix}, \text{ with } \omega_0 \geq 0, \tag{20}$$

the solution of the system can be immediately obtained by observing that

$$\tilde{z} = g/\sigma_0 s_\tau \tag{21}$$

satisfies the second equation (7) and the initial condition. Hence, substituting it in the first equation (6) yields

$$\dot{\omega}_z = -\sigma_1/J\omega_z + 1/J(\tau_e(t) - g s_\tau), \tag{22}$$

which is linear and has the closed-form solution

$$\tilde{\omega}_z(t) = e^{-\sigma_1/Jt}\omega_0 s_\tau + 1/J\int_0^t e^{-\sigma_1/J(t-\alpha)}(\tau_e(\alpha) - g s_\tau)\text{d}\alpha \tag{23}$$

that is obviously of the same sign s_τ of $\tau_e(t)$ and it is limited if the external torque is limited since (22) is asymptotically stable. Denote this limit with Ω. The following proposition holds.

Proposition 2. The solution $\tilde{z}(t)$ as in (21), $\tilde{\omega}_z(t)$ as in (23) of the dynamic system (6) and (7) with initial conditions (20) is locally asymptotically stable for any $|\tau_e(t)| > g$ $\forall t \geq 0$ if $\Omega < \frac{\sigma_0 g}{4J\sigma_1}$.

Proof. We will present the proof for $s_\tau = -1$ (thus $\tilde{\omega}_z(t) \leq 0$ $\forall t \geq 0$), which is the case considered in the experiments of Section 4, but the case $s_\tau = +1$ is similar. The jacobian of the linearized system around the nominal solution is

$$\boldsymbol{A}(t) = \begin{pmatrix} -\sigma_1/J & -\sigma_0/J \\ 0 & \sigma_0/g\tilde{\omega}_z(t) \end{pmatrix}.$$

In view of the assumption $|\omega_z(t)| \leq \Omega < \frac{\sigma_0 g}{4J\sigma_1}$, it is

$$4\sigma_1\sigma_0/(Jg)|\tilde{\omega}_z(t)| - \sigma_0^2/J < 0, \ \forall t \geq 0$$

and thus

$$\boldsymbol{A}(t)^T + \boldsymbol{A}(t) < 0, \ \forall t \geq 0.$$

Therefore, in view of Theorem 7.2 in (Rugh, 1996), the linearized system is uniformly asymptotically stable and thus the nominal solution of the nonlinear system is locally asymptotically stable.

Remark 3. Considering the typical values of the parameters of such a model (see Tab. 1 in Section 4), the assumption on the bound of $\tilde{\omega}_z(t)$ is not conservative at all. Moreover, in case of time varying maximum torque $g(t)$, if it is sufficiently smooth, the solution $\tilde{z}(t) = g(t)/\sigma_0$ is very close to the actual solution, the closer the larger is σ_0.

In conclusion, the control problem is solvable only if $|\tau_e(t)| > g(t)\ \forall t \geq 0$ and the desired velocity profile $\omega_d(t)$ has to be selected with a sign equal to that of $\tau_e(t)$.

3.2 Nonlinear observer

The control strategy discussed in the next subsection is aimed at designing a suitable normal force f_n such that the given velocity profile $\omega_d(t)$ is followed as close as possible. We assume that no other sensor is available except a force/torque sensor able to measure the full contact wrench in (3). Therefore, it is necessary to estimate the angular velocity $\omega_z(t)$. This problem can be solved only if the observability condition holds for the dynamic model (6) and (7) with the output equation

$$y = h(\omega_z, z) = \sigma_0 z + \sigma_1 \omega_z, \tag{24}$$

that is the total friction force measured by the sensors on the fingertips. A property of the dynamic system at hand will be necessary, the so-called *boundedness* property.

Proposition 4. For any τ_e such that $|\tau_e| < g$, the rectangle

$$\mathcal{Z} = \left\{ (\omega_z, z) \in \mathbb{R}^2 : \ |z| \leq \frac{g}{\sigma_0},\ |\omega_z| \leq \frac{g}{\sigma_1} \right\} \tag{25}$$

is positively invariant (i.e., all the solutions starting in $\mathcal{Z}$ remain in $\mathcal{Z}$) and asymptotically attractive, i.e. $\lim_{t\to\infty} \left| \left(\omega_z^T, z^T\right)^T \right|_{\mathcal{Z}} = 0$, while for any bounded $|\tau_e| > g$ the rectangle

$$\mathcal{Z}_\tau = \left\{ (\omega_z, z) \in \mathbb{R}^2 : \ |z| \leq \frac{|\tau_e|}{\sigma_0},\ |\omega_z| \leq \frac{|\tau_e|}{\sigma_1} \right\} \tag{26}$$

is positively invariant.

Proof. Define the quadratic function

$$V(\omega_z, z) = \frac{1}{2}\left(\frac{\sigma_0}{J} z^2 + \omega_z^2\right) \tag{27}$$

that is positive definite and proper, so it can be used as Lyapunov function candidate. Its time derivative along the trajectories of the system (6) and (7) is

$$\dot{V}(\omega_z, z) = -\frac{\sigma_0^2 z^2}{Jg}|\omega_z| + \frac{\tau_e}{J}\omega_z - \frac{\sigma_1}{J}\omega_z^2.$$

In the case $|\tau_e| > g$, $\dot{V}$ is negative both when $|z| > \frac{|\tau_e|}{\sigma_0}$ and when $|\omega_z| > \frac{|\tau_e|}{\sigma_1}$, and in this case $\mathcal{Z}_\tau$ is asymptotically attractive. The case $|\tau_e| < g$ is analogous.

We are now ready to prove observability.

Proposition 5. Let $\mathcal{M} \subset \mathbb{R}^2 = \{(\omega_z, z) \in \mathbb{R}^2 : \ \omega_z > 0\}$, then the system (6), (7) and (24) is locally weakly observable (Hermann and Krener, 1977) at any initial state $(\omega_z(0), z(0)) \in \mathcal{M}$.

Proof. The thesis holds if and only if the following matrix has rank 2 $\forall (\omega_z, z) \in \mathcal{M}$ (Nijmeijer and van der Schaft, 1990)

$$\Theta(\omega_z, z) = \begin{pmatrix} dh(\omega_z, z) \\ \mathcal{L}_f^1 dh(\omega_z, z) \end{pmatrix}$$

where dh represents the gradient of the function $h(\omega_z, z)$ and $\mathcal{L}_f^i$ is the Lie derivative operator of order i along the vector function $\boldsymbol{f}(\omega_z, z)$ whose components are the second members of the equations (6) and (7). This matrix for $(\omega_z, z) \in \mathcal{M}$ is

$$\Theta(\omega_z, z) = \begin{pmatrix} \sigma_1 & \sigma_0 \\ -\frac{\sigma_1^2}{J} + \sigma_0\left(1 - \frac{\sigma_0}{g} z\right) & -\frac{\sigma_0}{J}\sigma_1 - \frac{\sigma_0^2}{g}\omega_z \end{pmatrix}$$

that is full rank for $\omega_z > 0$ owing to the boundedness property. In fact, its determinant is

$$-\sigma_0^2 - \sigma_0^2/g(\sigma_1\omega_z + \sigma_0 z)$$

that cannot be zero since $\omega_z < g/\sigma_1$ and $z < g/\sigma_0$. The same result holds for $\omega_z < 0$ by considering the domain $\mathcal{M}' = \{(\omega_z, z) \in \mathbb{R}^2 : \ \omega_z < 0\}$.

Given the observability property, the nonlinear observer

$$\dot{\widehat{\omega}}_z = \frac{l}{J}\left(-\sigma_0 \widehat{z} - \sigma_1 \widehat{\omega}_z + y\right),\ l > 0 \tag{28}$$

$$\dot{\widehat{z}} = \widehat{\omega}_z - \frac{\sigma_0}{g}\widehat{z}|\widehat{\omega}_z| \tag{29}$$

$$\widehat{y} = \sigma_0 \widehat{z} + \sigma_1 \widehat{\omega}_z. \tag{30}$$

can be used to estimate the velocity ω_z. The structure of the observer is the same of the original dynamic system with the measured output y playing the same role of the external torque τ_e, but with an inertia moment scaled by the observer gain l. The higher the gain, the faster is the convergence. As soon as $|y| > g$, the observer has the same stability properties of the system. Note that y is the generalized measured torque w.r.t. the CoR and can be computed from finger sensor as (Costanzo et al., 2020)

$$y = \tau_n - c f_t. \tag{31}$$

3.3 Control law

The idea at the basis of the control law consists in reducing the normal force to allow a controlled motion of the slider while avoiding falling of the manipulated object at the same time, i.e., executing the so-called pivoting maneuver, but with the objective to follow a given velocity profile.

The design is based on the dynamic model presented so far. Assuming that the object has been grasped in a configuration such that an external torque, the gravity, has constant sign, and that the normal force f_n is designed in a way such that $|\tau_e| > g(f_n, c)$, then we know from Section 3.1 that ω_z has constant sign as well and that $\sigma_0 z = g\text{sign}(\omega_z)$. Thus the dynamic system is reduced to the first order equation (22), where the control input is in the argument of g and the dependence is nonlinear. Therefore, we consider the dynamics of the system linearized around the nominal motion (21) and (23). To compute the jacobian of equation (17) with respect to f_n, in view of (9) and (10), it can be re-written in the form

$$g(f_n, c) = \mu\delta f_n^{\gamma+1}(\xi|\tilde{\tau}_{n_{LS}}| + |\tilde{c}\tilde{f}_{t_{LS}}|) \simeq \mu\xi\delta f_n^{\gamma+1}, \tag{32}$$

assuming that $\tilde{c} << 1$, that means also $\tilde{\tau}_{n_{LS}} \simeq 1$. In other words, we are assuming that moments are prevailing on linear forces, that is a necessary for execution of the pivoting maneuver.

Thus, the new control input u is the variation with respect to a constant normal force $\bar{f}_n$ which is the minimum

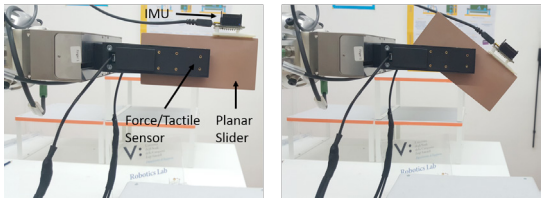

Fig. 2. Experimental setup: before sliding (left) and after sliding (right).

grasping force which does not allow slipping and it is computed according to the model presented in Section III.B of (Costanzo et al., 2020). The linearized dynamics, with a slight abuse of notation, is

$$\dot{\omega}_z = -\sigma_1/J\omega_z + \beta/Ju + 1/J\tau_e, \tag{33}$$

where

$$\beta = \left.\frac{\partial g}{\partial f_n}\right|_{f_n=\bar{f}_n} = \mu\xi\delta(\gamma+1)\bar{f}_n^{\gamma}. \tag{34}$$

The design of the control algorithm has to take into account also some implementation details, such as the digital interface of the gripper that has a sampling rate of 50 Hz and the lag time introduced by the low-level force control, that is approximately 0.120 s. Then a simple loop shaping method is adopted to obtain good stability margins. The resulting control algorithm is a simple PID-like, i.e., the transfer function,

$$C(s) = \frac{k_c}{s}\frac{1+sT_{11}}{1+sT_{12}}\frac{1+sT_{21}}{1+sT_{22}}, \quad \text{with } k_c > 0,\ T_{ij} > 0. \tag{35}$$

In conclusion, assuming a negative desired velocity (case $s_\tau = -1$), the normal force is computed as

$$f_n = \bar{f}_n + C(\omega_d - \hat{\omega}_z), \tag{36}$$

where C is the integro-differential operator corresponding to the transfer function in (35). Note that if a positive desired velocity is set ($s_\tau = +1$), k_c should be negative.

4. EXPERIMENTS

To show the effectiveness of the velocity observer and the control law, two experiments have been carried out.

Figure 2 shows the experimental setup. The experiments are carried out by using an industrial gripper WSG-50 by Weiss Robotics equipped with the SUNTouch six-axis force/tactile sensors described in (Costanzo et al., 2019) and based on the technology originally proposed by De Maria et al. (2012). The sensor can measure the full contact wrench and it has a serial interface with a sampling frequency of 500 Hz for all six components. The gripper is force-controlled via a feedback loop closed on the normal load f_n measured by the sensors that controls the velocity of the fingers. The digital control loop can run only at 50 Hz due to the limitation imposed by the communication architecture of the gripper. Moreover, the low-level velocity control loop is not able to actuate reference velocities lower than 5 mm/s, hence affecting the performance of the overall control system.

The gripper is used to grasp a resin block far from its CoG such that the gravity moment is about 0.015 Nm. An ST iNemo Inertial Measurement Unit (IMU) is attached to the block to measure the actual angular velocity ω_z.

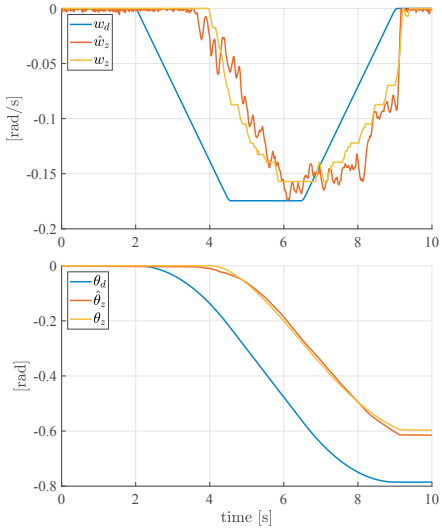

Fig. 3. Experiment 1: Desired, measured and estimated velocities (top) and angular positions (bottom).

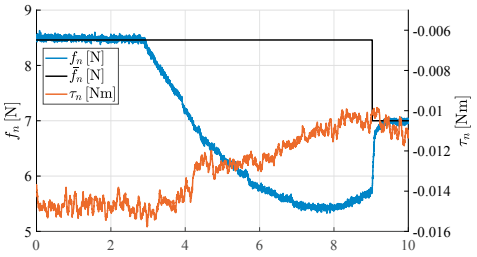

Fig. 4. Experiment 1: Control input f_n (left-axis) and measured external torque (right-axis).

In both experiments, the objective is to let the object rotate in-hand to reach the position in Fig. 2 right. To do that, a trapezoidal velocity profile is used as reference velocity ω_d for the control law described in Section 3.3. Moreover, at the same time, the angular velocity is measured by the IMU and estimated by the nonlinear observer described in Section 3.2. The model parameters used in the experiments, and shown in Tab. 1 together with the chosen control parameters, have been experimentally identified.

System Parameter	Value	Control Parameter	Value
J	$3.77 \cdot 10^{-4}$ kgm^2	k_c	20 N/rad
σ_0	50 Nm/rad	T_{11}	2.639 s
σ_1	0.02 Nms/rad	T_{12}	8.681 s
μ	0.58	T_{21}	$5.081 \cdot 10^{-1}$ s
γ	0.3	T_{22}	$7.53 \cdot 10^{-2}$ s
δ	0.004 m/N$^\gamma$		

Table 1. Experimentally identified system parameters and control parameters.

In the first experiment, the controller (36) is closed directly on the velocity measured by the IMU. In other words (36) is computed by using ω_z instead of $\hat{\omega}_z$. Figure 3 shows the result. The top plot shows the reference trajectory ω_d, the real and estimated velocity ω_z and $\hat{\omega}_z$. The bottom plot shows the angular positions (computed as integral of the velocities). Finally, Fig. 4 shows the control signal f_n, the force component $\bar{f}_n$ and the external torque measured by the tactile sensor τ_n that goes towards lower values

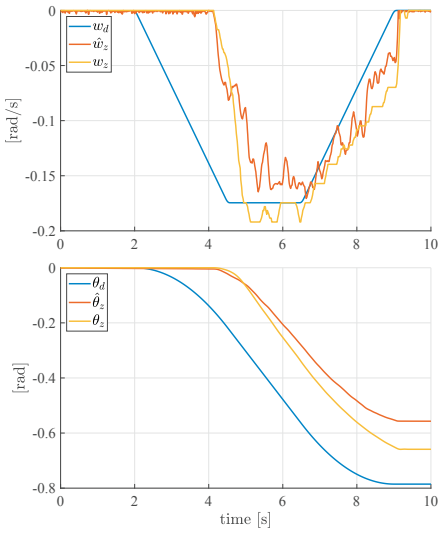

Fig. 5. Experiment 2: Desired, measured and estimated velocities (top) and angular positions (bottom).

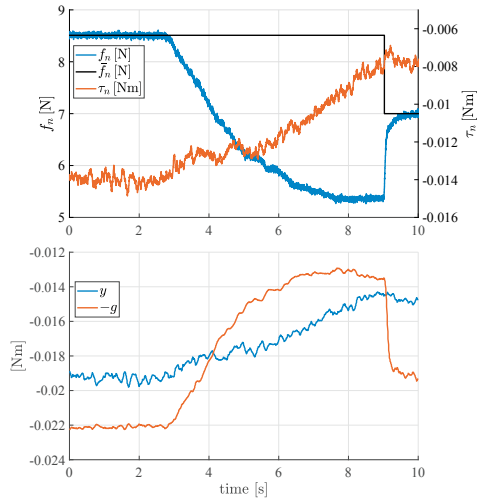

Fig. 6. Experiment 2: Control input f_n (top-plot left-axis) and measured external torque (top-plot right-axis); relation between the maximum dry friction torque g and the generalised measure y (bottom)

during the experiment. $\bar{f}_n$ is kept constant during the pivoting maneuver and it is updated when the reference ω_d goes to zero. The experiment clearly shows how the observer is able to capture the velocity measured by the IMU. The large initial tracking error is caused by the 5 mm/s threshold of the low-level velocity control loop. Nevertheless, the error of the observer keeps limited. Thus, using the estimated velocity to close the loop is reasonable.

In the second experiment, the estimated velocity $\hat{\omega}_z$ is used to close the control loop. Figures 5 and 6 show the results, that are very similar to those of the previous experiment. This demonstrates how the algorithm is still stable when using $\hat{\omega}_z$ in the control loop. Figure 6 (bottom) shows the relation between the maximum dry friction torque g and the generalised measure y defined in (31). When g is greater than y (in terms of absolute values), no velocity is generated by the observer because the dry friction can counteract the external torque. Instead, between 4 and 9 seconds, g is lower than y, thus the observer generates the observed velocity shown in Fig. 5 (top).

5. CONCLUSION

The paper presented a control strategy to allow robots equipped with parallel gripper and tactile sensors to rotate objects in hand without re-grasping maneuvers. The method regulates the grasping force based on an sliding velocity estimated via a nonlinear observer. Applications can be envisaged in the pick-and-place tasks.

REFERENCES

Canudas de Wit, C., Olsson, H., Aström, K.J., and Lishinsky, P. (1995). A new model for control of systems with friction. *IEEE Trans. on Aut. Control*, 40(5), 419–425.

Costanzo, M., De Maria, G., and Natale, C. (2018). Slipping control algorithms for object manipulation with sensorized parallel grippers. In *2018 IEEE Int. Conf. on Robotics and Automation*, 7455–7461. IEEE.

Costanzo, M., De Maria, G., and Natale, C. (2020). Two-fingered in-hand object handling based on force/tactile feedback. *IEEE Transactions on Robotics*, 36(1), 157–173. doi:10.1109/TRO.2019.2944130.

Costanzo, M., De Maria, G., Natale, C., and Pirozzi, S. (2019). Design and calibration of a force/tactile sensor for dexterous manipulation. *Sensors*, 19(4).

Dafle, N., Rodriguez, A., Paolini, R., Tang, B., Srinivasa, S., Erdmann, M., Mason, M., Lundberg, I., Staab, H., and Fuhlbrigge, T. (2014). Extrinsic dexterity: In-hand manipulation with external forces. In *2014 IEEE Int. Conf. on Robotics and Automation*, 1578–1585. Hong Kong.

De Maria, G., Natale, C., and Pirozzi, S. (2012). Force/tactile sensor for robotic applications. *Sensors and Actuators A: Physical*, 175, 60 – 72.

Goyal, S., Ruina, A., and Papadopulous, J. (1991). Planar sliding with dry friction, part i. limit surface and moment function. *Wear*, 143, 307–330.

Hermann, R. and Krener, A. (1977). Nonlinear controllability and observability. *IEEE Transactions on Automatic Control*, 22(5), 728–740.

Howe, R. and Cutkosky, M. (1996). Practical force-motion models for sliding manipulation. *The International Journal of Robotics Research*, 15(6), 557–572.

Lynch, K. and Park, F. (2017). *Modern Robotics: Mechanics, Planning, and Control*. Cambridge University Press, New York.

Nijmeijer, H. and van der Schaft, A. (1990). *Nonlinear Dynamical Control Systems*. Springer-Verlag.

Piazza, C., Grioli, G., Catalano, M., and Bicchi, A. (2019). A century of robotic hands. *Annual Review of Control, Robotics, and Autonomous Systems*, 2(1), 1–32.

Rugh, W. (1996). *Linear System Theory*. Information and System Sciences. Prentice Hall, 2nd edition.

Viña, F., Karayiannidis, Y., Smith, C., and Kragic, D. (2016). Adaptive control for pivoting with visual and tactile feedback. In *2016 IEEE Int. Conference on Robotics and Automation*, 399–406. Stockholm, SE.

Xydas, N. and Kao, I. (1999). Modelling of contact mechanics and friction limit surfaces for soft fingers in robotics, with experimental results. *The Int. Journ. of Robotics Research*, 18, 941–950.